Journal of Sound and Vibration (1998) **211**(4), 617–636

PARAMETRIC IDENTIFICATION OF VORTEX-INDUCED VIBRATION OF A CIRCULAR CYLINDER FROM MEASURED DATA

C. F. CHRISTENSEN

Ramboll, *Bredevej* 2, *DK* 2830, *Virum*, *Denmark*

AND

J. B. ROBERTS

School of Engineering, *University of Sussex*, *Falmer*, *Brighton*, *Sussex*, *BN*1 9*QT*, *England*

(*Received* 3 *June* 1997, *and in final form* 10 *November* 1997)

A non-linear, single-degree-of-freedom model is developed to describe the vortex-induced, transverse vibration of a circular cylinder, elastically suspended in a wind flow. The model is appropriate for predicting the dynamic response during lock-in conditions. The "linear-in-the parameters" nature of the model allows the formulation of a relatively simple and computationally very efficient procedure for estimating all the unknown parameters in the model. The method, based on the use of a state variable filter, enables the parameters to be estimated recursively by processing digitized records of the cylinder dynamic response. The technique is validated by applying it to both simulated data, where the parameters are known *a priori*, and to real data obtained from an experimental rig placed in a wind tunnel. For the experimental data, which relates to time-varying wind flow conditions, representing the natural wind, it is shown that the estimation technique allows the response during lock-in events to be isolated and treated separately. A reasonably good fit to the experimental data is obtained and the resulting estimates of the mean values of the parameters are found to converge satisfactorily.

1. INTRODUCTION

Steady wind flow around a fixed circular cylinder will result in vortex shedding over a wide range of Reynolds number with a frequency, ω_s, that is, by and large, proportional to the far field velocity. This vortex shedding produces a fluctuating transverse force on the cylinder. Thus, if the cylinder is elastically suspended, such that it is free to vibrate in a transverse direction, a resonant vibration will occur when the vortex shedding frequency is close to the natural frequency of the cylinder and its suspension system, ω_n.

It is well known that transverse vibration can lead to significant changes in the surrounding flow. Under suitable conditions the vortex shedding becomes much more coherent, and "locked-in" to the cylinder vibration, with $\omega_s \approx \omega_n$, over a rather wide range of wind velocity, resulting in a significant increase in the magnitude of the fluctuating transverse force. Thus there is a feedback effect during lock-in which can lead to large amplitude vibration (e.g., see references [1, 2]). This aero-elastic phenomenon is important in structural wind engineering because its occurrence may induce fatigue damage at "hot spots" in wind exposed tubular structures.

If the wind flow is not steady the wind velocity varies continuously, and randomly, with time and hence ω_s also tends to vary randomly. When ω_s approaches ω_n a lock-in event

0022–460X/98/140617 + 20 $25.00/0/sv971393

can occur with the amplitude building up rapidly, due to the feedback phenomenon. Such an event can last for many cycles, during which time ω_s becomes synchronized with ω_n, to a close approximation, and the vibration is almost sinusoidal, with a slowly varying amplitude. The lock-in event ceases when the wind velocity changes to the extent that synchronization can no longer be maintained. Thus the dynamic response to a non-steady (e.g., turbulent) wind can be regarded as a random process. In a typical realization, or sample function, of this process lock-in events appear as randomly occurring bursts of high amplitude vibration, within a background of much lower level random vibration. Since the time taken for the vibration to decay after a lock-in can be appreciable, the decay may not be completed before the next lock-in event occurs. Thus, depending on the frequency with which they occur, the lock-in events may appear to overlap each other to some extent.

In this paper attention is focused on modelling the dynamic behaviour during the lock-in events which occur randomly when the flow is turbulent. For this purpose a simple, single-degree-of-freedom model is adopted. Previous studies (e.g., [3–5]) have shown that such models may be adequate for the purposes of predicting the response amplitude. On the basis of data acquired under steady flow conditions a specific linear-in-the-parameters model is formulated. It is shown, through an analysis of both simulated and real experimental data, that the parameters in the model can be successfully estimated in a recursive fashion by applying a state-variable estimation method to dynamic response data. For the experimental data the estimation technique allows the data relating to lock-in events to be isolated and treated separately.

For the experimental data discussed here both the size of the test cylinder and magnitude of the turbulence intensity is significantly greater than in the experiments of most previous workers. For example, as regards cylinder size, the cylinder used by Goswami *et al*. [4] was one quarter of that in the present work. The turbulence intensity in most experiments reported in the literature is usually very small, and may be considered negligible: in contrast, in the present experimental work, the turbulence level is similar to that found in the natural wind and is a very important factor.

2. THE EQUATION OF MOTION

2.1. THE GENERAL FORM

The system under consideration is shown schematically in Figure 1. It consists of a circular cylinder, of diameter D and length L, immersed in a fluid of density ρ. The fluid velocity, in a direction orthogonal to the cylinder axis, is $U = \bar{U} + u$, where $\bar{U}$ is the mean velocity and u is a fluctuation with respect to the mean. The cylinder is suspended

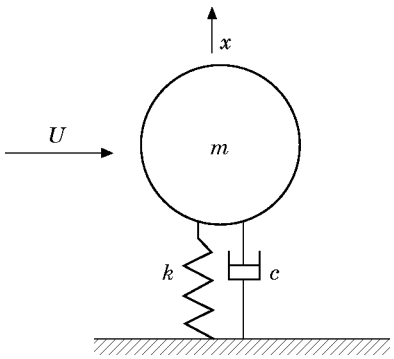

Figure 1. Elastically supported cylinder with transverse airflow.

elastically such that it is free to vibrate transversely, in the direction x. It is assumed that the suspension can be represented as a linear spring, of stiffness k, in parallel with a linear viscous damper, with coefficient c.

Since only transverse motion is under consideration the governing equation of motion may be written as

$$m(\ddot{x} + 2\zeta\omega_n\dot{x} + \omega_n^2 x) = F(t) = \tfrac{1}{2}\rho U^2 DLf(t), \tag{1}$$

where

$$\zeta = 0{\cdot}5c/\sqrt{km}, \qquad \omega_n^2 = k/m \tag{2}$$

and m is the mass of the cylinder. Here ζ is the usual non-dimensional damping ratio and ω_n is the undamped natural frequency. $F(t)$ represents the fluid induced transverse force. Since, for the experiments to be discussed later, the fluid medium is air the fluid inertial force, $m_0\ddot{x}$, where m_0 is the added mass, is assumed to be negligible. As indicated in equation (1), the fluid force is non-dimensionalized, as $f(t)$, through the introduction of the dynamic pressure, $\rho U^2/2$ and the transverse area DL.

The simplicity of equation (1) is deceptive since the real modelling difficulties arise in the mathematical representation of the scaled fluid force, $f(t)$. This will depend not only on the flow velocity but also on the history of the motion of the cylinder, in a complex and non-linear way.

Previous studies (e.g., [4, 5]) have indicated that, during lock-in conditions, when the amplitude of motion is relatively high and approximately sinusoidal, the fluid force can be adequately represented as a function of the instantaneous motion of the cylinder. This motion can be expressed in terms of

$$X = x/D, \qquad Y = \dot{x}/U, \tag{3}$$

where X, Y are, respectively, a non-dimensional displacement and velocity. Thus

$$f(t) = f(X, Y, \boldsymbol{\lambda}), \tag{4}$$

where $\boldsymbol{\lambda}$ is an n-vector of parameters: i.e.,

$$\boldsymbol{\lambda} = [\lambda_1, \lambda_2, \ldots, \lambda_n]^{\mathrm{T}}. \tag{5}$$

In general the values of the parameters will depend on the wind velocity. If the fluid force is such that there is negative overall damping at small amplitudes and a positive overall damping at high amplitudes then limit cycles will occur. The amplitude of these cycles may be determined from the condition that the total energy dissipation in one cycle is zero.

For the purpose of analysis it is very convenient, for the reasons discussed in section 3, to adopt a linear-in-the-parameters form for $f(t)$. A suitable such form, for the present purposes, is

$$f(t) = \lambda_1 g_1(X, Y) + \cdots + \lambda_{n-1} g_{n-1}(X, Y) + \lambda_n X. \tag{6}$$

Here the first $n - 1$ terms model the energy dissipation and the last term represents an aerodynamic stiffness. The first term in equation (6) will be assumed to be linear with respect to velocity: i.e.,

$$g_1(X, Y) = Y. \tag{7}$$

Combining equations (1) and (6) one obtains an equation of motion of the form

$$\ddot{x} + 2\zeta\omega_n\dot{x} + h(x, \dot{x}, U) + \omega_m^2(U)x = 0, \tag{8}$$

where

$$h(x, \dot{x}, U) = \sum_{i=1}^{n-1} \mu_i U^2 g_i(X, Y) \tag{9}$$

is a non-linear damping term and

$$\omega_m^2(U) = \omega_n^2 + \mu_n U^2/D, \qquad \mu_i = -\rho D L \lambda_i / 2m, \qquad i = 1, \ldots, n. \tag{10}$$

For limit cycles to occur one expects that $\mu_1 U + 2\zeta\omega_n < 0$ and at least one of the remaining damping parameters to be positive.

In the case of a turbulent wind the variation of U with time introduces a significant level of complexity into the model. If the turbulence intensity, $\sigma/\bar{U}$ (where σ is the r.m.s. of u), is appreciably less than unity then the equation of motion can be considerably simplified by assuming that U may be replaced by $\bar{U}$. Then equation (8) reduces to

$$\ddot{x} + 2\zeta\omega_n \dot{x} + h(x, \dot{x}) + \omega_m^2 x = 0, \tag{11}$$

where

$$h(x, \dot{x}) = \sum_{i=1}^{n-1} \alpha_i g_i(X, Y), \tag{12}$$

$$\omega_m^2 = \omega_n^2 + \alpha_n/D, \qquad \alpha_i = \mu_i \bar{U}^2, \qquad i = 1, \ldots, n. \tag{13}$$

In the experimental work to be discussed later the turbulence intensity was about 20%.

An example of this linear-in-the-parameter model is the Van der Pol representation, used by a number of researchers (e.g., see reference [2]). Here $n = 3$ and

$$h(x, \dot{x}) = \alpha_1 Y + \alpha_2 X^2 Y. \tag{14}$$

Clearly, here $g_2(X, Y) = X^2 Y$.

2.2. DETERMINATION OF THE DAMPING TERM

An appropriate form for the fluid damping term can be determined through processing experimental data, relating to constant wind velocity, to obtain the variation of the response amplitude with time, during a lock-in event. Here it will be assumed that the structural damping term, $2\zeta\omega_n\dot{x}$, in equation (11) is negligibly small, compared to the fluid damping. In fact, this represents no loss of generality since, if the structural damping is not negligible then the form deduced will be applicable to the combined damping contributions.

The amplitude, $a(t)$, and phase, $\varphi(t)$, of the response can be *defined uniquely* by the relationships

$$x(t) = a \cos \phi, \qquad \dot{x}(t) = -a\omega_m \sin \phi, \tag{15}$$

where

$$\phi = \omega_m t + \varphi. \tag{16}$$

Transforming equation (11) into amplitude and phase variables one obtains a first order differential equation for the amplitude, as follows:

$$\dot{a} = (1/\omega_m) h(a \cos \phi, -a\omega_m \sin \phi) \sin \phi. \tag{17}$$

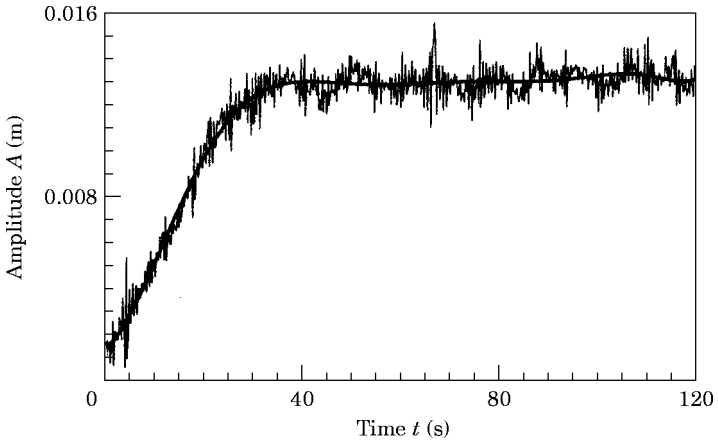

Figure 2. Response amplitude versus time for constant wind velocity. The thick line is a polynomial of ninth degree fitted to the measured amplitude.

If the damping is light then both a and φ are constant over one cycle, to a good approximation: in these circumstances, following the method of Kryloff and Bogoliubov (e.g., [6]) the right side of this equation may be averaged over one cycle to give

$$\dot{a} = (1/\omega_m)H(a), \tag{18}$$

where

$$H(a) = \frac{1}{2\pi}\int_0^{2\pi} h(a\cos\phi, -a\omega_m \sin\phi)\sin\phi \, \mathrm{d}\phi. \tag{19}$$

$H(a)$ is proportional to minus the rate of energy dissipation with respect to time. Thus, using the assumption that φ is approximately constant over one cycle, one has, from equation (16), $\mathrm{d}\phi = \omega_m \, \mathrm{d}t$ and hence

$$\oint h(x, \dot{x}) \, \mathrm{d}x = \oint h(x, \dot{x})\dot{x} \, \mathrm{d}t = -aH(a). \tag{20}$$

Equation (18) shows that if the derivative of a, as deducted from measured data, is plotted against a then an estimate of the function $H(a)$ is obtained.

Figure 2 shows a typical variation of amplitude, a, with time during a lock-in event. The data was obtained from the experiments described in section 6 with a nominally constant wind velocity. There is a relatively small, high frequency component, due to the turbulence in the wind tunnel, which had an intensity of about 4·0%. If the data is smoothed by fitting a polynomial function then, as shown in Figure 2, the amplitude rises monotonically from an initially low level to the limit cycle amplitude, which is almost constant.

If the derivative of the smoothed amplitude shown in Figure 2 is plotted against amplitude the curve shown in Figure 3 is obtained. According to equation (18), this curve is proportional to the function $H(a)$. The estimated $H(a)$ function rises to a maximum value and then falls to a small fluctuation about zero, at the limit cycle amplitude. The overall variation is reasonably well represented by a fifth order polynomial of odd order, as shown in Figure 3. Thus

$$H(a) = \gamma_1 a + \gamma_2 a^3 + \gamma_3 a^5, \tag{21}$$

where the parameters γ_1, γ_2 and γ_3 were found by fitting equation (21) to the estimated function, in a least squares sense. At small amplitudes the first term in equation (21) is dominant and $H(a)$ rapidly increases, and linearly, with increasing amplitude. The parameters of the remaining two, non-linear terms, γ_2, γ_3, are both negative and these terms become dominant at high amplitudes.

For the present purposes a form for $h(x, \dot{x})$, corresponding to equation (21), is needed. The mapping from $H(a)$ to $h(x, \dot{x})$ is not unique: a wide variety of forms for $h(x, \dot{x})$ will yield the same form of $H(a)$. For example, both

$$h(x, \dot{x}) = \alpha_1 Y + \alpha_2 Y^3 + \alpha_3 Y^3 \tag{22}$$

and

$$h(x, \dot{x}) = \alpha_1 Y + \alpha_2 X^2 Y + \alpha_3 X^4 Y \tag{23}$$

will give the form of $H(a)$ given in equation (21). It is noted that the first two terms in equation (23) correspond to the Van der Pol model for damping (see equation (14)).

For lightly damped systems the precise form of the damping function $h(x, \dot{x})$ is not important provided that the variation of the rate of energy dissipation with amplitude is correct. Thus here the simple velocity dependent form given by equation (22) is chosen. The linear term this equation can include the structural damping contribution, since $2\zeta\omega_n\dot{x} \propto Y$.

The damping form given by equation (22) may still be appropriate in the case a time-varying wind but the parameters can be expected to vary randomly from one lock-in event to another. This variation may be attributed, at least in part, to changes in the wind velocity, U, (see equations (9) and (10)) but other factors, such as the effect of initial conditions at the beginning of a lock-in event, may also be important. In the present paper it will be assumed, in the main, that the *mean* values of the parameters can be estimated by treating them as constants, when fitting models to the data. However, some attempt is also made to estimate the variation of the parameters, across a sequence of lock-in events.

2.3. THE PARAMETRIC FORM OF THE EQUATION OF MOTION

On combining equations (11) and (22) one obtains the following linear-in-the-parameters, parametric form for the equation of motion, referred to henceforth as Model A:

$$\ddot{x} + a_1\dot{x} + a_2\dot{x}^3 + a_3\dot{x}^5 + px = 0. \tag{24}$$

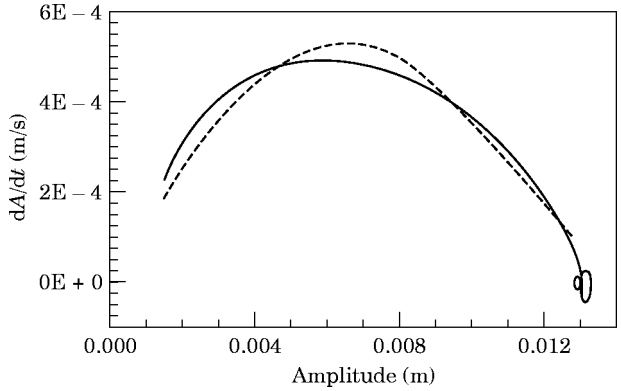

Figure 3. The derivative of the amplitude versus the amplitude. The dashed curve was obtained by fitting a fifth degree polynomial of odd order terms.

Here

$$a_1 = 2\zeta\omega_n + \alpha_1/\bar{U}, \qquad p = \omega_m^2 = \omega_n^2 + \alpha_4/D, \tag{25}$$

$$a_2 = \alpha_2/\bar{U}^3, \qquad a_3 = \alpha_2/\bar{U}^5. \tag{26}$$

In this approach one inherently assumes that the parameters may be treated as constants, for the purpose of estimating their mean values, as discussed above. It is also assumed that U may be approximated by $\bar{U}$ (see section 2).

Some allowance for the effect of the time variation of U may be made by using equation (8) rather than equation (11): i.e., replacing α_i by $\mu_i U^2$ and using U rather than $\bar{U}$. Instead of equations (24) to (26) one then has

$$\ddot{x} + b_1(U)\dot{x} + b_2(U)\dot{x}^3 + b_3(U)\dot{x}^5 + p(U)x = 0, \tag{27}$$

where

$$b_1 = 2\zeta\omega_n + \mu_1 U, \qquad p = \omega_n^2 + \mu_4 U^2/D, \tag{28}$$

$$b_2 = \mu_2/U, \qquad b_3 = \mu_3/U^3. \tag{29}$$

This model will be referred to henceforth as model B. Again the mean values of the parameters in this model can be found by treating them as constants, when fitting the model to the data.

3. PARAMETRIC IDENTIFICATION

The following parametric identification problem will now be addressed: how can sample functions of the response process, $x(t)$, over some period of time 0-T, be processed to yield estimates of the mean values of the parameters (a_1, p, a_2, a_3) in Model A, or the mean values of the parameters (b_1, p, b_2, b_3) in Model B? Here a solution to this problem will be developed for Model A, in some detail. The same method can be applied to Model B but, since the same basic steps are involved, details are omitted here.

Since the equation of motion is applicable only during lock-in events it is necessary to isolate these sections from the complete displacement record, when applying an estimation method. Lock-ins can be defined to begin when the amplitude starts to increase significantly and to stop when the amplitude starts to fall (see section 5). If the lock-in sections are spliced together, to form a new truncated record, there will inevitably be discontinuities at the joins which need to be accounted for.

The fact that the equation of motion is linear-in-the-parameters means that one is dealing with a *linear* estimation problem. This is a great advantage since linear estimation methods are, in general much simpler, and computationally more efficient, than non-linear methods.

Here a linear method, based on the state variable filter approach (e.g., see references [7, 8]), is employed. One of the basic ideas in this method is to move all the unknown parameters to the right side of the equation of motion so that the quantities associated with them can be treated as inputs to a known system. This can be achieved by adding $c_1\dot{x} + c_2 x$ to both sides to equation (24) and introducing the new parameters

$$f_1 = a_1 - c_1, \qquad f_2 = p - c_2. \tag{30}$$

On rearranging, the equation of motion becomes

$$\ddot{x} + c_1\dot{x} + c_2 x = -f_1\dot{x} - f_2 x - a_2\dot{x}^3 - a_3\dot{x}^5. \tag{31}$$

Here the parameters c_1, c_2 are filter parameters which are treated as *known* constants, which can be set to any desired values. Both c_1 and c_2 need to be positive to guarantee that the linear filter, represented by the left side of equation (31), is stable. In addition the filter parameters must be chosen so that the pass band of the filter encompasses the predominant frequencies in the system response.

With this rearrangement the unknown parameters are now f_1, f_2, a_2 and a_3. These need to be augmented by two further parameters, d_1 and d_2, to allow for non-zero initial conditions:

$$w_1 = x(0), \qquad w_2 = \dot{x}(0). \tag{32}$$

Thus the parameter vector of unknowns is

$$\boldsymbol{\theta}^{\mathrm{T}} = [f_1, f_2, a_2, a_3, d_1, d_2]. \tag{33}$$

To implement a linear estimation scheme it is useful to introduce four auxiliary functions, $y_1(t)$, $y_2(t)$, $y_3(t)$, $y_4(t)$, where

$$x = f_1\dot{y}_1 + f_2 y_1 + a_2 y_2 + a_3 y_3 + d_1\dot{y}_4 + d_2 y_4. \tag{34}$$

It follows, by substitution into equation (31), that equation (34) is a solution if the auxiliary functions satisfy the differential equations

$$\ddot{y}_i + c_1\dot{y}_i + c_2 y_i = v_i(t), \qquad i = 1, 2, 3, 4, \tag{35}$$

where

$$v_1 = -x, \qquad v_2 = -\dot{x}^3, \qquad v_3 = -\dot{x}^5, \qquad v_4 = 0. \tag{36}$$

If the initial conditions are set as

$$y_i(0) = \dot{y}_i(0) = 0, \qquad i = 1, 2, 3, \tag{37}$$

$$y_4(0) = 0, \qquad \dot{y}_4(0) = 1, \tag{38}$$

then the following relationships exist between d_1, d_2 and the initial conditions:

$$w_1 = d_1, \qquad w_2 = d_2 - d_1(f_1 + c_1). \tag{39}$$

Introducing matrix notation equation (34) can be written as

$$x(t) = \mathbf{X}^{\mathrm{T}}(t)\boldsymbol{\theta}, \tag{40}$$

where

$$\mathbf{X}^{\mathrm{T}}(t) = [\dot{y}_1, y_1, y_2, y_3, \dot{y}_4, y_4]. \tag{41}$$

The parameter vector can be estimated by minimizing the least-squares cost function

$$J = \sum_{i=0}^{N} [x(t_i) - \mathbf{X}^{\mathrm{T}}(t_i)\boldsymbol{\theta}]^2, \tag{42}$$

where it assumed that the response process is measured at times t_i.

Equation (42) is the basis for the least squares estimation method. The vector $\mathbf{X}(t_i)$ can be found by numerically solving equations (35) (for example, by using the fourth order Runge–Kutta algorithm) since $v_i(t)$ can be derived directly from the measured response.

It is possible to generate the parameter vector recursively, at each time step, by using the algorithm given in the Appendix. Discontinuities in the data, arising from splicing, can be fully accounted for, readily, in the recursive approach, by estimating the parameters d_1 and d_2 anew at the beginning of each section (see the Appendix). Since only d_1 and d_2 are re-estimated at each join, rather than all the parameters, the evolution of the system parameters is not interrupted by the joins, resulting in a very efficient estimation scheme.

TABLE 1

Final estimated system parameters for different time steps

	True values	Estimated $\Delta t = 0{\cdot}005$ s	Estimated $\Delta t = 0{\cdot}004$ s	Estimated $\Delta t = 0{\cdot}003$ s	Estimated $\Delta t = 0{\cdot}002$ s	Estimated $\Delta t = 0{\cdot}001$ s
a_1	−0·600	−0·756	−0·725	−0·693	−0·662	−0·630
p	767·3	766·9	767·0	767·1	767·1	767·2
a_2	0·70	0·830	0·805	0·778	0·751	0·729
a_3	0·50	0·263	0·309	0·355	0·402	0·433

By tracking the system parameters continuously, through each join, the degree of convergence obtainable for the whole, concatenated data record can be examined. If the blocks of data were simply processed separately then all the parameters would need to be re-estimated at each join, with loss of efficiency, and convergence of the systems parameters within each block would be uncertain.

4. ANALYSIS OF SIMULATED DATA

To test the estimation algorithm, with Model A, it was applied to some simulated data, obtained by numerically solving the governing equation of motion (equation (24)). Data was simulated for a duration of 60 s, with a time step of 0·004 s and a natural frequency, $f_m = \omega_m/2\pi$, of 4·41 Hz. This gives about 57 data points per cycle. The initial conditions were set to $\dot{x}(0) = 0$, $x(0) = 0{\cdot}01$ m and the parameters were chosen as follows: $a_1 = -0{\cdot}60$, $a_2 = 0{\cdot}70$ and $a_3 = 0{\cdot}50$. The two parameters c_1 and c_2 were set to 0·10 and 710, respectively. Thus the true values of the parameters in $\boldsymbol{\theta}$ are as given in Table 1. With this set of values the response was found to reach its steady state, limit cycle, amplitude after about 15 s.

Figures 4 show the evolution of the estimated values of the four system parameters, f_1, f_2, a_2, a_3, with time, as obtained by applying the recursive state variable filter method. Here

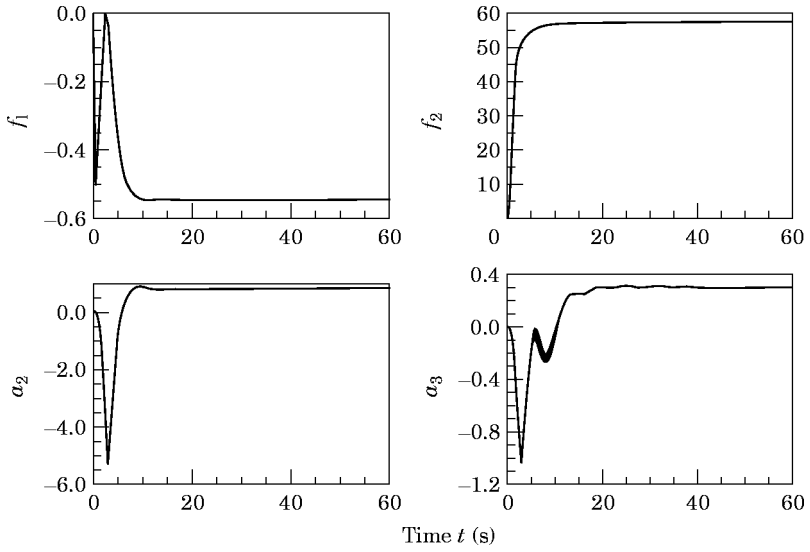

Figure 4. Variation of the four system parameter estimates with time: simulated data with no noise.

TABLE 2

Estimated values for different noise levels

	True values	Estimated $\sigma = 0{\cdot}01A$	Estimated $\sigma = 0{\cdot}02A$	Estimated $\sigma = 0{\cdot}05A$	Estimated $\sigma = 0{\cdot}10A$
a_1	−0·600	−0·730	−0·714	−0·734	−0·710
p	767·3	767·0	767·0	767·0	767·0
a_2	0·70	0·844	0·717	0·896	0·739
a_3	0·50	0·249	0·449	0·143	0·376

f_1 and f_2 are plotted, rather than a_1 and p: conversion is easily achieved by using equations (30). It is seen that the parameter estimates converge satisfactorily, stabilizing after about 30 s. However, the final estimates differ to some extent from the true values. These errors are due to numerical integration errors associated with the use of a finite time step and they reduce significantly if the time step is reduced, as shown by the results in Table 1 (in each case the simulated data consisted of 15 000 points). It is worth noting that, in all cases, an excellent fit to the data is obtained. The parameters a_2 and a_3 are the most difficult to estimate accurately; this is due to the fact that they "trade-off" against each other, so far as the representation of non-linear damping is concerned. Thus, whilst a_2 is overestimated, a_3 is underestimated with the effect that the true overall dissipation is accounted for correctly. To a lesser extent there is also a trade-off between the linear and non-linear damping parameters.

Experiments with splicing sections of simulated data together, and accounting for the resulting discontinuities by using the method outlined in the Appendix, gave very similar results to those in Table 1, thus validating the method of dealing with spliced data. However, the information content in data relating to the steady, low level response is relatively small so, if this kind of data predominates in a concatenated data set, the convergence may be much slower.

To test the influence of measurement noise of the accuracy of the estimation a sequence of independent, scaled Gaussian random numbers were added to the simulated data. This simulated the presence of a wide-band measurement noise. Table 2 shows some typical results for various noise levels. It can be seen that, in general, the estimation is not sensitive to the influence of noise, the parameters a_2 and a_3 (especially) being most affected. This is not surprising in view of the results in Table 1 and the estimates in Table 2 show again the trade-off between a_1, a_2 and a_3.

Figure 5 shows some typical evolutions of the parameter estimates with time in a case where simulated measurement noise is present ($\Delta t = 0{\cdot}004$ s). It can be seen that the principal effect of noise is to decrease the rate at which the parameters converge to stable values.

5. ANALYSIS OF MEASURED WIND TUNNEL DATA

5.1. EXPERIMENTAL FACILITY

The data used in the present paper was obtained from experiments carried out in a wind tunnel with a test section 1·75 m wide, 1·53 m high and 13·6 m long. Under steady flow conditions the turbulence intensity in the test section was approximately 4·0%. A fluctuating wind flow could be generated by sending appropriate signals to a wind generating propeller machine. These signals were simulated sample functions of a stationary Gaussian process with a non-zero mean and a prescribed power spectrum.

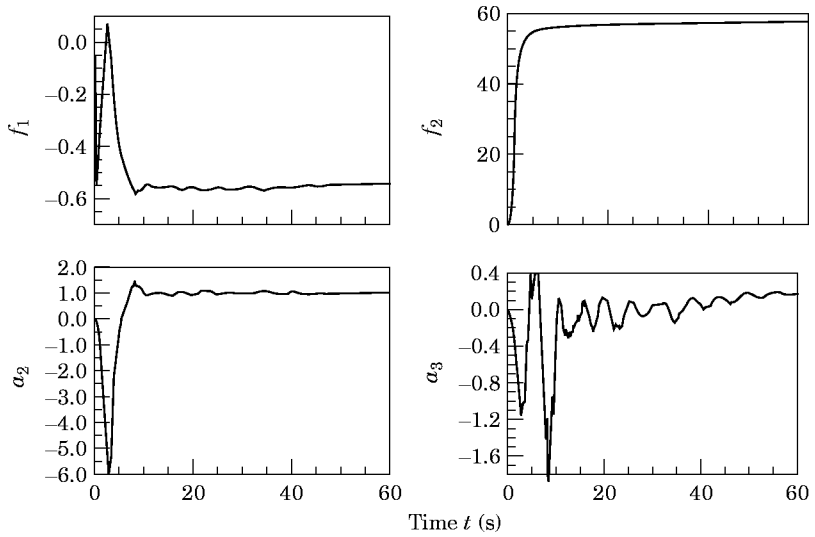

Figure 5. As Figure 4 but with added noise (standard deviation $\sigma = 0{\cdot}05A$).

The model was a circular Plexiglas cylinder with an outer diameter of 0·20 m and a length of 1·65 m. The cylinder was suspended horizontally on four springs allowing the model to oscillate in the vertical direction, orthogonal to the mean wind velocity vector. There was no arrangement to eliminate the along-wind vibrations but, because the load fluctuations in this direction are very small, these vibrations were in fact negligible. The mechanical mass of the oscillating system (cylinder, tubes, wires, transducers and added mass from the springs) was 13.3 kg. The model was positioned 11·6 m downstream of the end of the contraction. A diagram of the experimental set-up is shown in Figure 6.

For the experimental work a set of springs with an overall stiffness of 3·2 N/mm was chosen. Damping, in addition to that occurring naturally in the suspension system, was provided by magnetic means. Aluminum plates, 3 mm thick and 60 mm wide were attached to the ends of a rod mounted on the cylinder axis, as shown in Figure 6. The flow-induced vibration caused these plates to move between the poles of permanent magnets, thereby inducing eddy currents on the plate surfaces. The integrated effect of such eddy currents was a magnetomotive force proportional to, and directed opposite to, the cylinder velocity, thus providing viscous damping to the system. The magnitude of this damping force could be controlled by varying the size of the gap between the magnetic poles.

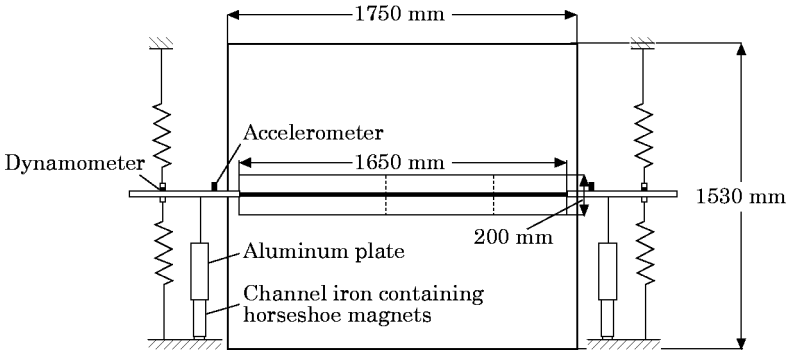

Figure 6. Cylinder suspension system, in elevation.

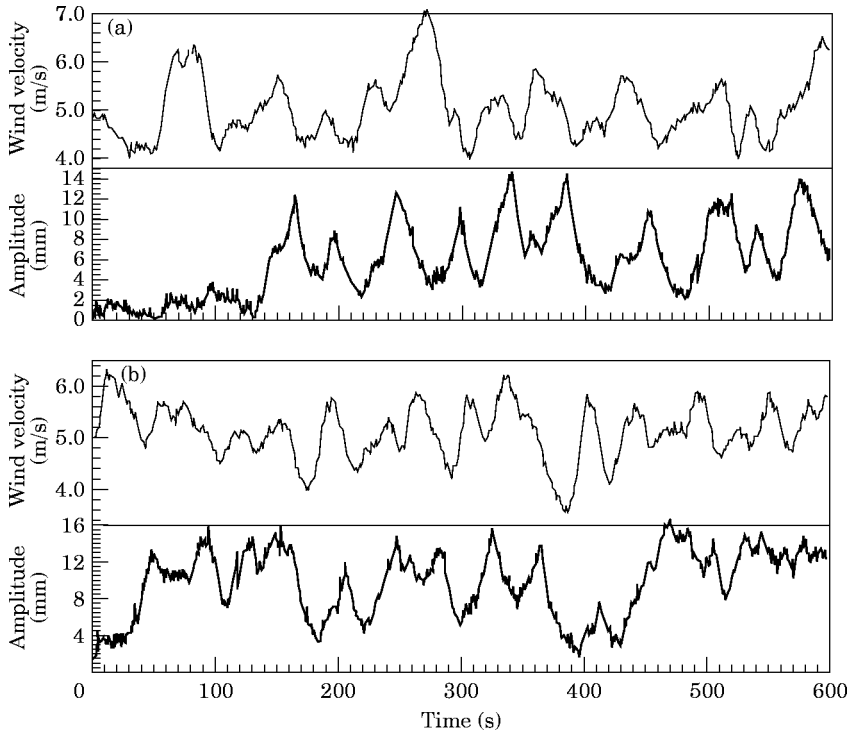

Figure 7. Experimental time histories. The upper curve in each figure is the wind far field velocity and the lower curve is the corresponding amplitude of the vibrating cylinder. (a) Case A; (b) Case B.

The accelerations of the cylinder were measured by two accelerometers placed at the ends of the cylinder: the velocity and displacement was obtained by integration. The wind velocity was measured by a hot-wire anemometer probe placed 1·0 m in front of the cylinder. The data was obtained by sampling the velocity and displacement measurements digitally at rates between 200 and 250 Hz.

5.2. EXPERIMENTAL DATA

All measurements analysed here were obtained by using the experimental facility described above. The natural frequency in still air was $f_1 = 4{\cdot}43$ Hz.

Figures 7 shows simultaneous variations of the measured far field wind velocity and the corresponding transverse cylinder displacement, in the case where a randomly fluctuating wind flow was generated. For the data in Figure 7(a) (case A) the structural damping ratio (ζ) was 0·47% and for the data in Figure 7(b) (case B) ζ was 0·31%; these values were estimated from free decay tests.

The data used for the estimation was determined on the basis of the variation of the cylinder vibration amplitude. A "lock-in" event was defined to begin when the amplitude started to increase and to stop where the amplitude started decreasing again. Figure 8 shows a typical lock-in event, identified by a visual inspection of the complete response record shown in Figure 7(a). It can be seen that the amplitude build-up is slow and that the start and end of the lock-in is reasonably well defined. For the present purposes the start and end were determined by eye. An alternative method of detecting the occurrence of a lock-in event is to check for coincidence of the vortex shedding frequency with the natural frequency of the system. However, the first method was preferred because the

measured amplitude represents the response to the average wind force over the entire length of the cylinder. In the second method the vortex shedding frequency could be inferred, in the present experiments, only from the pressure fluctuations at a few cross-sections.

For case A a concatenated data set consisting of nine such lock-in events was constructed (total number of data points 28 744; sampling rate 250·0 Hz). For case B the concatenated set consisted of eight "lock-in" events (total number of data points 27 273: sampling rate 200·3 Hz).

5.3. IDENTIFICATION BY USING MODEL A

Model A was fitted to these sets using the recursive identification method described in section 3. In Figures 9 the evolution of the system parameter estimates with time is shown, for both cases, again as obtained by using the state variable estimation method discussed in section 3. It is seen that the parameter f_2, corresponding to the stiffness, converges quickly, and that the estimates of the parameters corresponding to the damping, a_1, a_2 and a_3, are less stable. This behaviour is expected in view of the simulation results shown in section 4, which demonstrated the trade-off effect between these three parameters. Nevertheless, a reasonable degree of convergence is achieved, especially in Case A. Moreover, the model gives a very good fit to the data. Thus the predicted amplitude, during the estimation, nearly coincides with the measured data, as shown in Figures 10.

The estimates of the parameters are given in Table 3. From section 4 it is known that, for the sampling rates used here, the estimates of the parameters f_1 and a_2 are too large and the estimate of a_3 is too small. The simulation results given in Table 1 indicate that the parameters should be slightly corrected to allow for the error introduced by the relatively low sampling rate. The appropriate correction was found through an iterative process. Thus simulated data was generated with the sampling rate used in the experiments, and with parameter values equal to those estimated from the experimental data. The estimation errors incurred through the use of this sampling rate were then evaluated and the parameters adjusted iteratively until the simulation results coincided with the estimated from the experimental data. The corrected values are shown in brackets in Table 3.

Also shown in Table 3 are the estimated values of the fluid damping parameter

$$a_{1f} = a_1 - a_{1s} = a_1 - 2\zeta\omega_n, \tag{43}$$

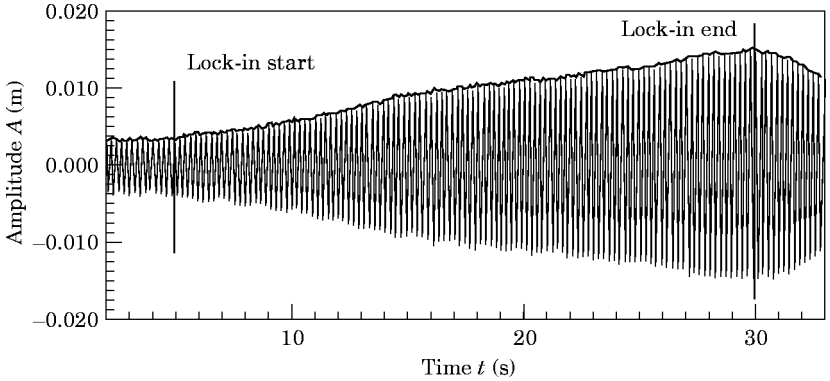

Figure 8. Definition of lock-in start and lock-in end.

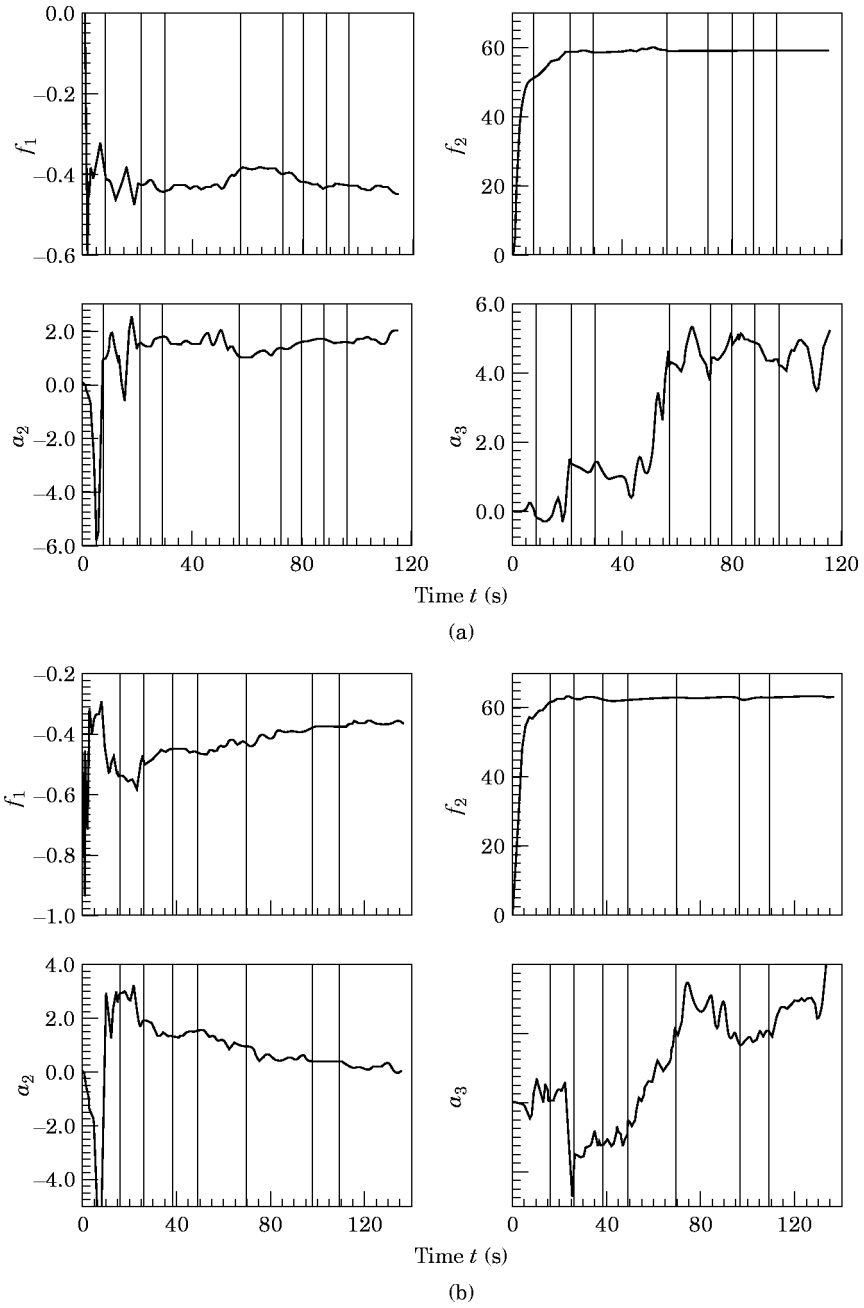

Figure 9. Evolution of the six parameter estimates with time. The vertical lines indicate where the data has been spliced together. (a) Case A; (b) Case B.

where a_{1s} is the structural damping contribution. Since the only difference between the Cases A and B is the level of structural damping it is perhaps surprising, at first sight, that the fluid damping parameters, a_{1f}, a_2 and a_3, are significantly different. However, if the total fluid damping force

$$f_f(t) = a_{1f}\dot{x} + a_2\dot{x}^3 + a_3\dot{x}^5 \tag{44}$$

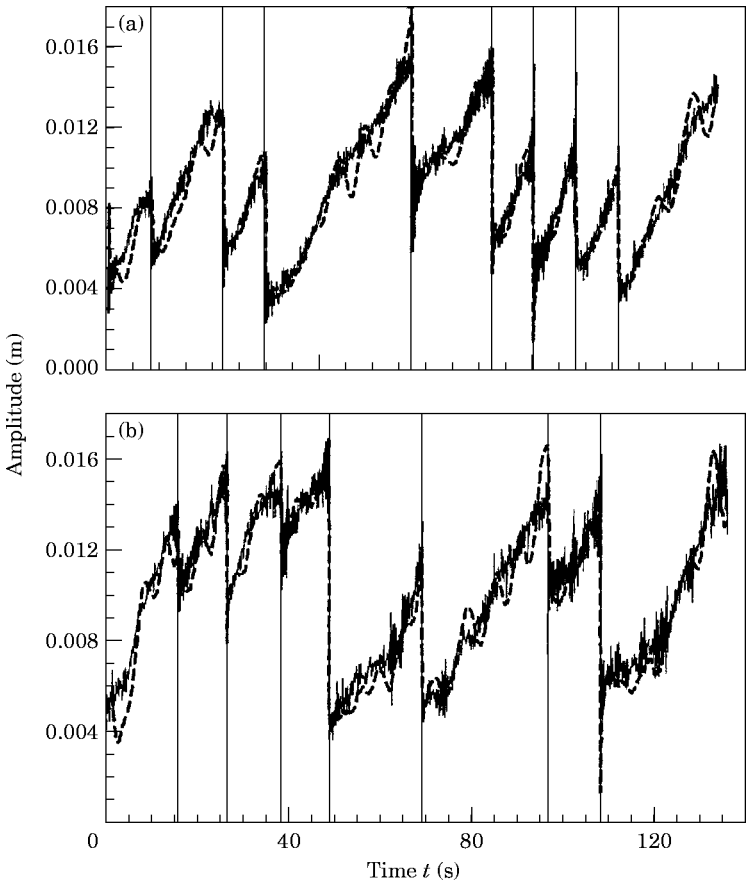

Figure 10. Comparison of the measured amplitude (solid line) with the estimated amplitude during the estimation (dashed line). (a) Case A; (b) Case B.

is plotted against $\dot{x}$, as in Figure 11, it can be seen that, for the range of velocity which encompasses the data, there is in fact a good agreement. Thus the trade-off errors of the individual parameters self cancel, to a large degree, when the overall damping level is considered.

It can also be seen from the results in Table 3 that the estimated natural frequency, f_m, is very close to the natural frequency of the system in still air. Thus wind motion has a negligible effect on the overall stiffness of the system (i.e., the value of the parameter α_4 is negligibly small).

TABLE 3

Final estimated system parameters obtained from experimental data

	a_1	a_{1f}	a_2	a_3	$p = \omega_m^2$	$f_m = \omega_m/2\pi$ (Hz)
Case A	−0·33	−0·59	1·6	4·5	769·2	4·41
corrected	(−0·27)	(−0·51)	(1·4)	(4·8)	–	–
Case B	−0·27	−0·44	0·30	2·8	772·4	4·41
corrected	(−0·17)	(−0·34)	(0·26)	(3·2)	–	–

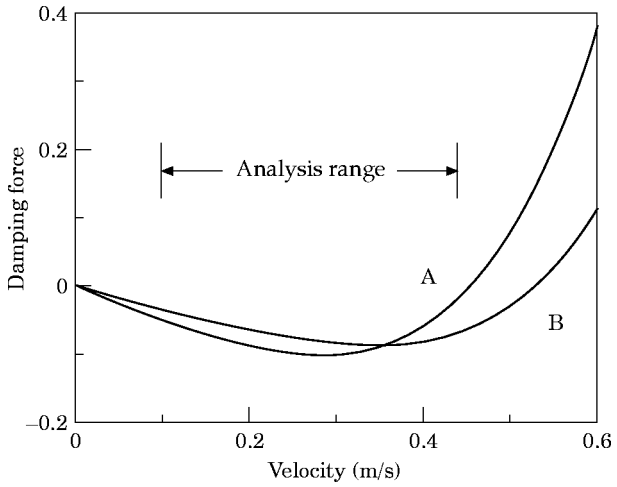

Figure 11. Variation of the damping force with velocity, for Cases A and B.

It is noted that, if the data sets are spliced together in different sequences the final estimates differ slightly but the general pattern of the results is preserved.

On solving the differential equation (24) with the corrected parameters, and the correct initial conditions the envelope shown in Figure 12 is obtained. This is seen to agree well with the measured amplitude. In contrast, the amplitude tends to become too large when the uncorrected estimated parameters are used. There is some systematic overprediction of the rate of growth of the displacement, especially in Case B, attributable to the inherent deficiencies in the model.

As pointed out earlier, one would expect the parameters to exhibit some degree of randomness and the estimates given in Table 3 are actually estimates of the mean values of the parameters. The present method allows for the possibility of estimating the parameters separately, *within* each lock-in event, rather than estimating them as common values across all the lock-in events. However, here the individual lock-in events are, in general, too short to obtain satisfactory estimates. This limitation is illustrated by the results shown in Figure 13. Here the parameter a_3 is estimated afresh during each event: thus a_3 is initialized, together with the initial conditions, at every join in the concatenated set. As seen from Figure 13 the estimated value of a_3 now fluctuates more but the time durations of the lock-in events are too short to obtain convergence.

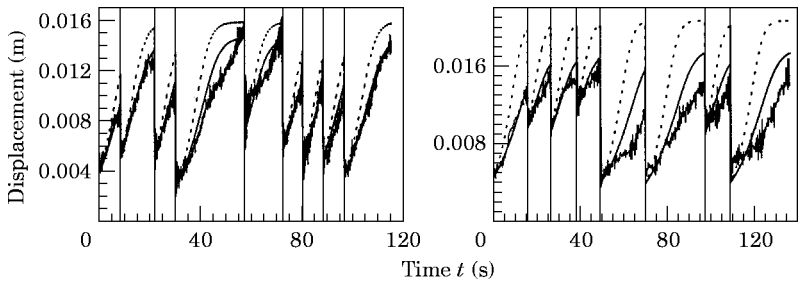

Figure 12. Comparison of the measured amplitude (solid line) with the amplitude estimated by using final parameter estimates. The dotted line is obtained when the estimated parameters are used and the smooth solid line is obtained when the corrected parameters are used. Left, Case A; right, Case B.

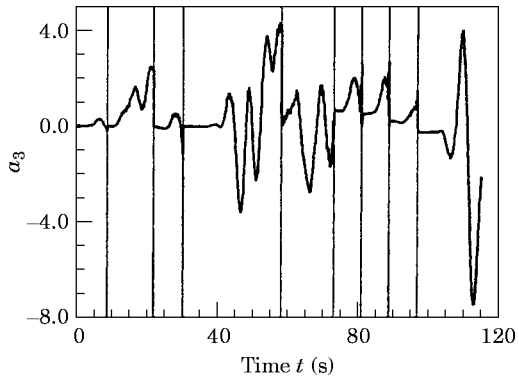

Figure 13. Evolution of the estimate of a_3 when it is initialized at each join; Case A.

If an equivalent logarithmic decrement and an asymptotic amplitude for the load model are calculated, and compared to the mean values found by Christensen and Ditlevsen [9], a reasonably good agreement is obtained.

5.4. IDENTIFICATION BY USING MODEL B

In principal Model B should be more accurate, since fewer approximations are involved.

If, in the light of the results obtained for Model A, the aerodynamic stiffness term, μ_4, is assumed to be negligible then the equation of motion for model B can be written as

$$\ddot{x} + c_1\dot{x} + c_2x = -f_1\dot{x} - f_2x - \mu_1(U\dot{x}) - \mu_2(\dot{x}^3/U) - \mu_3(\dot{x}^5/U^3), \tag{45}$$

where

$$f_1 = 2\zeta\omega_n - c_1, \qquad f_2 = \omega_n^2 - c_2. \tag{46}$$

Figures 14 show the evolution of the estimates of f_1, f_2, μ_1, μ_2 and μ_3 with time, as obtained by applying the recursive estimation method the experimental data (here case A). The overall level of fit is similar to that achieved with Model A and the estimation of the parameter, f_2, is again, very robust and accurate, giving an estimate of ω_n in close agreement with that found by using Model A. However, two unexpected features emerge in the estimation of the damping parameters. Firstly, the parameter f_1, although reasonably stable, does not converge to the value corresponding to structural damping (0·16). This suggests the presence of a simple linear aerodynamic term, as in Model A. Secondly the parameter μ_3 is very small and makes a negligibly small contribution. On this basis the fluid force can be represented by

$$F(t) = \kappa_1\dot{x} + \kappa_2(U\dot{x}) + \kappa_2(\dot{x}^3/U), \tag{47}$$

where κ_1, κ_2 and κ_3 are constants. However, on the basis of the data analyzed here (case B data gave similar results to case A) the representation given by equation (47) appears to offer no significant improvement over that used in Model A: i.e.,

$$F(t) = \eta_1\dot{x} + \eta_2\dot{x}^3 + \eta_3\dot{x}^5, \tag{48}$$

where η_1, η_2 and η_3 are constants.

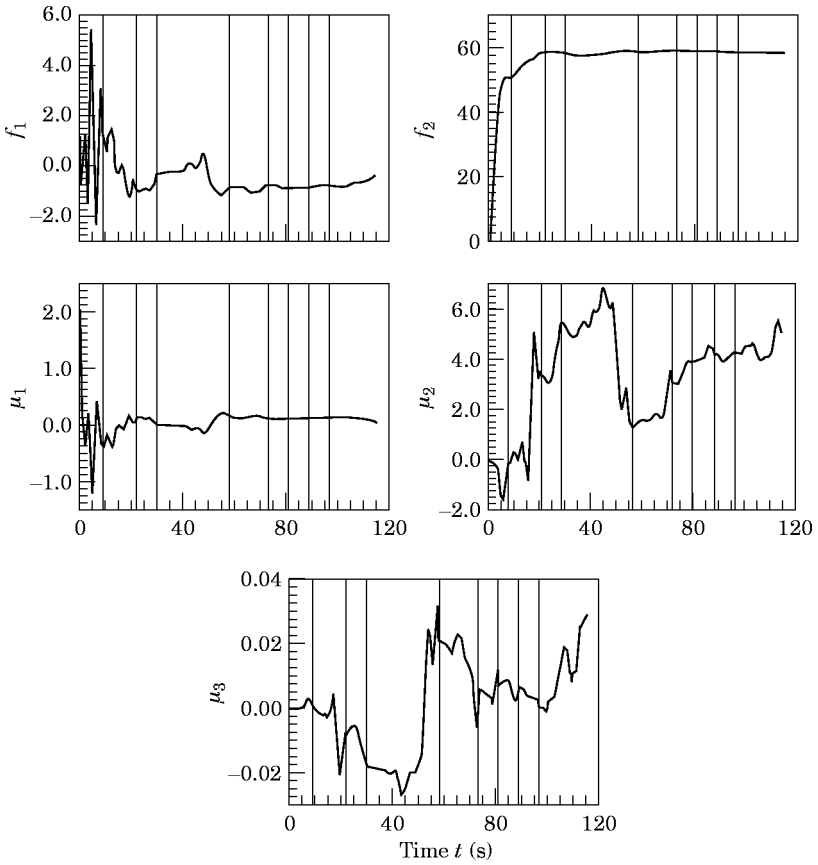

Figure 14. Evolution of the five system parameters with time; Model B, Case A. The vertical lines indicate where the data has been spliced together.

7. CONCLUSIONS

The main conclusions of this paper are summarized as follows.

1. A simple, single-degree-of-freedom, linear-in-the-parameters model can be used to describe the vibration response of an elastically suspended circular during "lock-in".

2. An appropriate form for the energy dissipation terms in the model can be derived from data relating to steady flow conditions by using the averaging method due to Kryloff and Bogoliubov.

3. A state variable filter method can be used to estimate all the parameters in the model, by processing measured displacement response histories during lock-in events. The method has been validated through simulation studies.

4. Application of the identification technique to measured wind tunnel data results in estimates of the mean values of the parameters which converge satisfactorily and give a reasonably good fit to the data.

5. The two model variants examined gave a similar degree of fit to the data, suggesting that there is no benefit in using the more complex one, which incorporates the time dependency of the wind fluctuation.

ACKNOWLEDGMENTS

This work was financially supported by the EU Human Capital and Mobility Programme "Stochastic Mechanics in Structural and Mechanical Engineering" and the Danish Technical Research Council, during a visit by the first author to the School of Engineering, University of Sussex, UK in 1996.

REFERENCES

1. T. Sarpkaya 1979 *ASME Journal of Applied Mechanics* **46**, 241–258. Vortex-induced oscillations: a selective review.
2. E. Simiu and R. H. Scanlan 1996 *Wind Effects on Structures*. New York: John Wiley. Third edition.
3. R. I. Basu and B. J. Vickery 1983 *Journal of Wind Engineering and Industrial Aerodynamics* **12**, 75–97. Across-wind vibrations of structures of circular cross-section, Part 2: development of a mathematical model for full scale application.
4. I. Goswami, R. H. Scanlan and N. P. Jones 1993 *Journal of Engineering Mechanics*, *ASCE* **119**, 2270–2287. Vortex-induced vibrations of circular cylinders. I: experimental data.
5. I. Goswami, R. H. Scanlan and N. P. Jones 1993 *Journal of Engineering Mechanics*, *ASCE* **119**, 2288–2302. Vortex-induced vibrations of circular cylinders. II: a new model.
6. J. B. Roberts and P. D. Spanos 1990 *Random Vibration and Statistical Linearisation*. Chichester, UK: John Wiley.
7. P. J. Gawthrop 1984 *Proceedings of the Institution of Electrical Engineers*, *Part D* **131**, 261–266. Parameter estimation from non-contiguous data.
8. P. J. Gawthrop 1984 *Journal of Mathematical Control and Information* **1**, 117–128. Parametric identification of transient signals.
9. C. F. Christensen and O. Ditlevsen 1996 Lock-in interval measurements and fatigue calculation of tubular structural elements subjected to wind (to be published).

APPENDIX

A suitable recursive least squares algorithm for the generation of estmates, $\hat{\boldsymbol{\theta}}_i$, of the parameter vector, $\boldsymbol{\theta}$, at each time step in the data, t_i, is summarized. The algorithm is very fast, since it avoids the need for matrix inversion.

At time t_i one computes the following:

(a) $$\mathbf{K}_i = \mathbf{P}_{i-1}\mathbf{X}_i/(1 + \mathbf{X}_i^{\mathrm{T}}\mathbf{P}_{i-1}\mathbf{X}_i); \tag{A1}$$

(b) $$\hat{\boldsymbol{\theta}}_i = \hat{\boldsymbol{\theta}}_{i-1} + \mathbf{K}_i[x_i - \mathbf{X}_i^{\mathrm{T}}\hat{\boldsymbol{\theta}}_{i-1}], \qquad \text{updated estimate;} \tag{A2}$$

(c) $$\varepsilon_i(\hat{\boldsymbol{\theta}}_i) = x_{i-1} - \mathbf{X}_i^{\mathrm{T}}\hat{\boldsymbol{\theta}}_{i-1}, \qquad \text{prediction error,} \tag{A3}$$

(d) $$\mathbf{P}_i = \mathbf{P}_{i-1} - \mathbf{K}_i\mathbf{X}_i^{\mathrm{T}}\mathbf{P}_{i-1}, \qquad \text{update of the covariance matrix.} \tag{A4}$$

It is necessary to initiate the calculation by setting an initial value to the covariance matrix, corresponding to high level of uncertainty. It is convenient to set

$$\mathbf{P}_0 = \alpha\mathbf{I} \tag{A5}$$

where $\mathbf{I}$ is the unit matrix and α is a large number.

At the first join, arising from splicing, the estimates of the parameters d_1 and d_2 in $\boldsymbol{\theta}$ are reset to zero. Those off-diagonal and diagonal elements of $\mathbf{P}$ relating to d_1 and d_2 are also reset to zero. All the other elements of $\mathbf{P}$ are retained at their values immediately preceding

the join. The recursive algorithm is then implemented until the second join is reached, where $\boldsymbol{\theta}$ and $\mathbf{P}$ are reset, as at the first join, and so on. A more detailed discussion and analysis of this procedure is given by Gawthrop [7]. If desired, other parameters can be re-estimated in each section by zeroing appropriate elements of $\boldsymbol{\theta}$ and $\mathbf{P}$ at the joins, in a manner similar to that described for d_1 and d_2.